

AUTOMATIC SEGMENTATION OF SPONDYLOLISTHESIS AND SCOLIOSIS OF X-RAY IMAGES USING LIGHT-WEIGHT RESUNET ARCHITECTURE

SHIVA PRASAD K¹, Dr. JANA S²

¹ Research scholar, Department of ECE, VelTech University, Avadi, Chennai, India

² Professor, Department of ECE, Vel Tech University, Avadi, Chennai,, India

E-mail: ¹vtd1061@veltech.edu.in, ²drsjana@veltech.edu.in

ABSTRACT

Scoliosis is the term for a curvature of the lumbar or thoracic spine in the coronal plane. Young children may develop spondylolisthesis and scoliosis, which, if left untreated, can grow into terrible agony. Lung and heart problems can also be caused by severe scoliosis. Early diagnosis can therefore help to arrest the disease's progression and make it easier to apply therapies or interventions. Recent research has focused on the use of convolutional neural networks for the diagnosis of scoliosis and spondylolisthesis on X-ray images. Unfortunately, the majority of the current approaches ignore the larger-scale image contextual feature information in favour of gathering feature information for prediction from localised parts of images. Furthermore, important features for classification—such as co-occurrence connections between labels and anatomical segmentation knowledge—are not completely utilised. This research suggests a Light-weight ResUNet (LW-RUNet) architecture that leverages the Xception backbone for feature extraction in order to segment scoliosis and spondylolisthesis using X-ray images. While the ResUNet decoder uses high-level features, the middle decoder uses middle features to get spatial information. To fine-tune the disease area, the suggested architecture integrates the ResUNet decoder characteristics with the proposed middle decoder features. The outcomes of the suggested segmentation technique are verified using a number of measures, including accuracy, sensitivity, IOU, and dice similarity coefficient. With regard to the normal, scoliosis, and spondylolisthesis classes, the suggested method's segmentation accuracy is 99.28%, 98.25, and 98.34, respectively.

Keywords: *Deep Learning, Scoliosis, Spondylolisthesis, Radiology, and X-ray images*

1. INTRODUCTION

Because of its benefits over non-ionizing radiation, cheap cost, and real-time capabilities, X-ray imaging is frequently employed in clinical settings for screening and diagnosing anatomical structures [1, 2]. X-ray imaging's drawback, however, is that radiologists' expertise and experience play a major role in the diagnosis process [3], which can lead to notable intra- and inter-individual variations. Significant advancements have been made in computer-aided medical image analysis methods for illness diagnosis and detection in recent years [4, 5]. Radiologists can diagnose patients more accurately and objectively by using these procedures. To successfully complete the goal tasks in medical analysis using supervised or semi-supervised learning methods [6], especially deep learning methods, large-scale labelled datasets are essential [7]. However, the quantity of pictures available for use in medical imaging tasks is restricted. This is

because annotating the data, which is a complicated and time-consuming procedure, requires medical experts with specialized understanding. Thus, the largest obstacle still facing the area of medical imaging is the dearth of large-scale annotated datasets. Through data augmentation, researchers have tried to address this issue by extending the dataset through the use of conventional affine transformations including rotating, flipping, cropping, and scaling. This technique can expand the sample size, but it adds no meaningful new information to the dataset and just modifies the image in a straightforward way [8]. Thus, there is an immediate need for a data augmentation technique that can increase the dataset's variability.

With the use of big medical datasets, researchers have advanced Deep Learning (DL) methods for classifying medical images considerably in recent decades. One of the most widely used disease imaging modalities for diagnosing the heart and lungs, X-ray (XR) imaging is a quick, painless method of screening for diseases that exposes the

patient to a wealth of visual diagnostic information with little radiation. It is also essential for the screening, diagnosis, and treatment of many diseases that can be fatal. Chest radiography picture data is readily available each year, but precise and efficient screening techniques are also needed for these images. However, the prolonged working time of X-ray radiographic screening, the resemblance of abnormalities in X-ray images to visual cues, and the shortage of experts to analyses X-ray radiographic images make accurate and efficient image analysis and illness detection challenging. Therefore, in order to assist medical professionals in accurately identifying abnormal chest X-rays during clinical routine, it is imperative that computer-aided and interpretable decision support systems be developed[9-10].

Multiple sclerosis (MS) is an autoimmune inflammatory disease of the central nervous system that affects the brain and spinal cord (SC). Early-stage atrophy usually requires cross-group comparisons, whereas early-stage demyelinating lesions are readily seen on magnetic resonance imaging (MRI), even in a single patient. The majority of MRI research on MS has focused on the brain, despite the fact that the SC contributes to disability [11]. SC MRI is more challenging to interpret than brain MRI because of the SC's smaller anatomical size than the brain and its greater sensitivity to artefacts. Moreover, neurodegeneration is a widespread illness affecting the brain and spinal cord. Diffuse neurodegeneration occurs in the grey matter, and in the white matter that seems normal, axonal loss occurs. These changes eventually result in severe shrinkage and loss of brain tissue, which is most apparent as the illness worsens[12-13].

Scoliosis is a three-dimensional malformation of the spine that is characterised by rotation of the vertebrae within the curve and a lateral curvature of more than 10 degrees. It can be classified as idiopathic, neuromuscular, or congenital. Based on when symptoms first appear, idiopathic scoliosis (IS) can be further classified into three age groups: infantile (birth to two years), juvenile (three to nine years), and adolescent (ten years and older) (Figure 1). The most prevalent musculoskeletal condition in children that results in a three-dimensional (3D) spinal deformity is this one [14-15]. Because the deformity comprises not only displacement and rotation in the frontal plane but also axial rotation of the vertebrae, it is always three-dimensional. Because the spinal deformity manifests during

times of substantial physical growth, adolescent IS is the most prevalent kind [16-17].

Spondyloarthritis (SpA) is a general term for any inflammatory joint disease involving the vertebral column. The most common of these disorders, ankylosing spondylitis (AS), is marked by ongoing inflammation of the joints and ligaments that run the length of the spine. The sacroiliac joints (SI joints), which connect the base of the spine to the pelvis, are typically also impacted by AS. Among the first signs are stiffness in the lower back and pain from inflammation. Fused vertebrae would eventually limit movement and increase the risk of fractures if the condition is not treated [21-22]. Complete fusion of the spinal vertebrae might eventually cause total joint damage, necessitating joint replacement [21]. Men are affected by AS more frequently than women and usually manifests before the age of 45. Usually, it first appears when a person is quite young. AS is a part of a broader category of illnesses called axial spondyloarthritis (AxSpA). AxSpA can be categorised as radiographic or non-radiographic based on whether radiographic imaging reveals alterations to the spine and sacroiliac joints[23]. Finding these kinds of radiological anomalies can help distinguish AS from radiographic AxSpA. Additionally, part 2 expounds upon associated research studies. Section 3 describes the suggested work in depth and also addresses fusion, selecting the best choice, and database definition. Extensive classification results are provided in Section 4. Lastly, Section 5 presents the study's conclusion. Examples of scoliosis in adolescents are shown in Figure 1.



Figure 1: A) Normal; B) Juvenile Idiopathic; And C) Severe Left Thoracic Adolescent Scoliosis.

The major contributions of the proposed method is

i) Light-weight ResUNet (LW-RUNet) architecture for the Segmentation of scoliosis and spondylolisthesis using X-ray images, which uses the Xception backbone for feature extraction.

ii) ResUNet decoder uses high-level features, the middle decoder uses middle features to recover spatial information. To fine-tune the disease area, the suggested architecture combines the ResUNet decoder characteristics with the suggested middle decoder features.

iii) Our research achieves great accuracy in terms of test accuracy, validation accuracy, and F1 score in three classes: scoliosis, spondylolisthesis, and normal spine, with respective percentages of 99.00%, 97.86%, and 97.86%. Additionally, pairwise classification has a high success rate of up to 99.57%.

iv) Our research proposes a comprehensive model for classifying vertebral X-ray images, which includes a dataset of X-ray images of normal vertebrae, scoliosis, and spondylolisthesis. As a result, it can be used simply by an expert to aid in X-ray picture recognition and classification.

2. RELATED WORK

According to the literature, Imaging the spine requires radiography, commonly known as X-rays. It provides a basic picture, giving a general overview of the anterior-posterior (AP)/posterior-anterior (PA) and lateral (LAT) potential projections. Although efforts have been made over the years to limit the amount of time people are exposed to X-rays, spine X-rays were once very often obtained. Between 1935 and 1965, the incidence of breast cancer almost doubled [18–19]. Children must have at least 12 x-rays taken during their adolescence, either during or after a diagnosis, even if radiation dosages are currently lower. Unfortunately, cumulative X-ray exposure puts children at several times the risk of cancer that adults do. Advancements in technology and computerisation have made optoelectronic techniques possible for the localisation of posture and body static disorders. Unfortunately, the most valuable advantage of X-rays is still the capacity to see morphological changes in the vertebrae and calculate the angle of torsion using the Cobb method. As previously mentioned, an X-ray is a radiation-intensive examination, so the diagnosis is usually delayed. Medical personnel cannot precisely determine if the anticipated results are attained or whether the applied treatment method is carried out correctly. As a result, computer

diagnostic techniques are the most effective diagnostic instrument due to their accuracy, non-invasiveness, and lack of X-ray side effects [20]. A primary contribution of the suggested approach is Xception is the backbone used for feature extraction in the Light-weight ResUNet (LW-RUNet) architecture for the segmentation of scoliosis and spondylolisthesis utilising X-ray images. While the ResUNet decoder uses high-level features, the middle decoder uses middle features to get spatial information. To fine-tune the disease area, the suggested architecture integrates the ResUNet decoder characteristics with the proposed middle decoder features.

Number of machine learning studies have been released for the purpose of classifying and segmenting X-ray pictures. For instance, Jeon et al. used ResNet and Faster R-CNN to classify images of patient spines. The Area Under the Curve score of 90.87% [10] fully illustrates how the combination of the ResNet convolutional neural network and Faster R-CNN has a stronger classification effect on scoliosis disorders than traditional machine learning techniques. Additionally, Radaelli et al. used Mask RCNN in combination with the YOLOv5 approach for vertebral localization to segment the spinal column. The final average classification accuracy of the proposed technique is 94.69% [11]. That being said, since many radiologists who examine CT images are not educated in musculoskeletal radiology, subtle indicators of early-stage AS, including erosion, may go undetected. A further effect of typical ageing is a degenerative alteration in the sacroiliac joint that causes localised fusion, a disorder that resembles AS symptoms.

General radiologists might identify AS in its early stages from CT scans with the use of an automated diagnostic tool that could differentiate between early AS and the AS-like symptoms associated with ageing[20]. Medical image analysis has already witnessed the outstanding performance of Deep Learning based approaches. On the other hand, the majority of application scenarios—such as the segmentation of lung nodules, the automatic classification of tuberculosis, and the identification of COVID-19—usually only involve one particular kind of illness or lesion. Nevertheless, it is possible for several diseases to coexist in an XR image, in which case it becomes more difficult to precisely detect and identify the co-existing disorders. Classifying different chest diseases from XR

images is a hot research issue at the moment, as it is a multi-label classification challenge .

Mahiba et al. classified spondylolisthesis or normal using the MobileNet model in a Convolutional Neural Network, achieving excellent results [14]. Additionally, 229 X-ray images—156 with spondylolisthesis and 143 with a normal spine—were gathered by Jones et al. and optimized using the TFLite model optimization technique. The model achieves a high accuracy rate as a result, including 98% for the VGG16 model and 96% for the InceptionV3 model [15]. Furthermore, Wang et al. used GoogleLeNet and AlexNet models to categorize the 272 X-ray pictures in the data set. Experimental results show that GoogleLeNet has a 93.87% accuracy rate, which is somewhat better than AlexNet's 91.67% accuracy [16].

3. METHODOLOGY

This section offers a concise overview of the primary processing frameworks in this paper. It includes the generator and discriminator structures' complete convolution structures as well as the introduction of a combined loss function that reduces category imbalance. Deep convolutional neural networks have made significant advancements in the automatic segmentation of spondylolisthesis and scoliosis. The robustness of autonomous feature extraction in those methods has allowed them to significantly surpass older methods in segmentation performance. However, maintaining the stringent assumption that the training and test datasets have the same distribution is one of the most important things. Hospitals usually obtain medical datasets from different suppliers using different scanner procedures, which leads to differences in appearance distribution discrepancies (also known as domain shifts).

On the testing set with this kind of distribution difference, the majority of research showed that well-trained CNNs' segmentation performance had significantly declined. One common approach to resolving domain shift problems is unsupervised domain adaptation, which reduces the distribution disparities between domains by learning domain-invariant features or generative adversarial networks. Conversely, current unsupervised domain adaptation methods usually need a sufficient amount of easily accessible datasets from the target domain in order to be trained. The requirement might not be achievable due to the restricted quantity of target domains and the unpredictability

of target domain alterations. Figure 2 illustrates the constructed network's overview.

A simplified version of the ResUNet architecture is the suggested Lightweight ResUNet architecture. Several levels of the Xception architecture have been used in place of the residual blocks in the encoder section. The training dataset was used to train the Xception architecture, which is provided in the library. A middle decoder and the residual decoder of the ResUNet architecture are combined to retrieve spatial resolution. While the suggested middle decoder employs the encoder's mid-level features to gather more information about the x-ray picture dataset, the residual decoder uses high-level features to learn spatial information.

The skip connections are used to concatenate the feature maps of the two decoders. The findings of the second experiment, which demonstrates how to use the middle decoder to effectively minimise the wrong area and aid in boundary refinement. Figure (2) shows the planned architecture's structural layout. It should be noted that the transferred weights from the pre-trained Xception architecture are used as initial weights in the proposed architecture. This is done for a few reasons: first, the pre-trained Xception architecture's weights are retrained in the scoliosis and spondylolisthesis segmentation task due to low dataset similarity. To improve the suggested architecture's capacity for generalization: The transfer learning technique improves the suggested architecture's capacity for generalization on the unseen dataset. The essential components of the suggested LW-RUNet architecture are described in detail below.

3.1. Residual Block

In this work shows that each residual block is made up of two streams: the activation function and the batch normalisation (BN) layer along with the feature extractor path, which has multiple (3×3) convolution layers with a stride of 1, and the skip connection path [13], which has a (1×1) convolution layer with a stride of 2. The combined outputs from the two pathways are added. With a skip link, the input X is available and passed to the subsequent layers, allowing the network to deepen and converge more quickly without having to worry about the vanishing gradient issue. The overall block diagram of the proposed method is given in Figure 3.

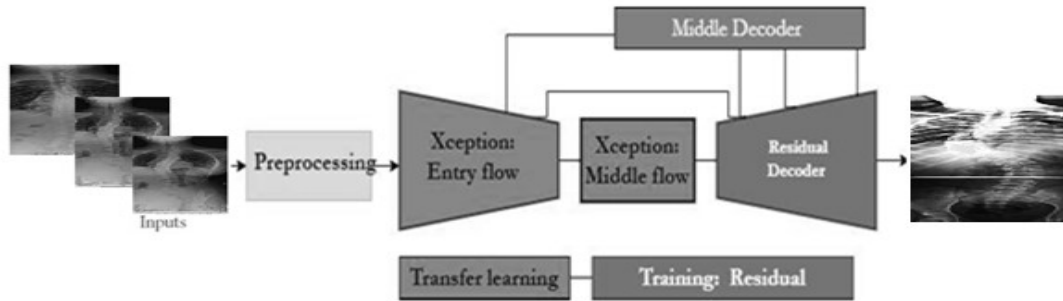


Figure 2. Proposed model block diagram

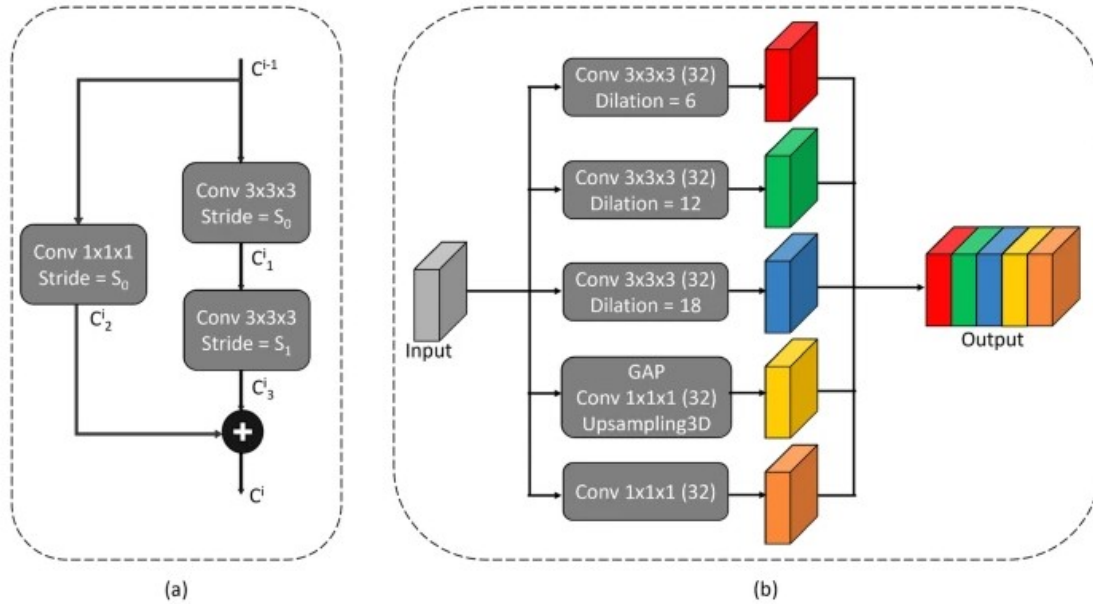


Figure 3. The principal block architecture of the suggested LW-ResUnet architecture.

3.2.Xception Architecture

Xception reduces time and space complexity by employing a linear stack of depth-wise separable convolution layers with residual connections. Chollet [11] suggests this architecture for segmentation issues. This architecture makes use of Depthwise Separable layers, a subset of the Inception network. As demonstrated in Figure 4, Depthwise Separable initially learns the correlation between the input channels using (1×1) convolutional layers. Next, it uses (3 × 3) convolutional layers to learn spatial correlation in each of the output channels independently. A notable benefit of this layer over the more established conventional layer is the substantial decrease in computations. Three main flows

comprise the Xception architecture [11]: an entering flow, a middle flow, and an exit flow. A block is a stack of Depthwise Separable layers, and each flow consists of many blocks. The Xception architecture is more efficient than the Inception design, based on the findings reported in [11]. Depthwise Separable blocks allow for the efficient use of network parameters, which reduces computations and leads to greater efficiency. Additionally, they demonstrated how using residual structure helps the network and classifier's accuracy to converge more quickly. Therefore, the encoder portion of the suggested architecture uses a portion of the Xception architecture. To keep the network parameters from over-increasing, the

suggested LW-UNet design solely uses entry and intermediate flows to extract the feature.

4. EXPERIMENTAL RESULTS AND DATA SET

4.1 Data set

The King Abdullah University Hospital at the Jordan University of Science and Technology in Irbid, Jordan, is where the local vertebral X-ray pictures were obtained. The vertebral X-ray pictures are accessible to the public at <https://www.kaggle.com/datasets/yasserhessein>. Table 1 lists the three classifications that make up the data set: normal, spondylolisthesis, and scoliosis. The dataset utilised in this work is split into two parts: 70% of the data are used for training and 30% are used for testing.

Figure 4. The Principal Block Architecture Of The Suggested Lw-Xception Architecture.

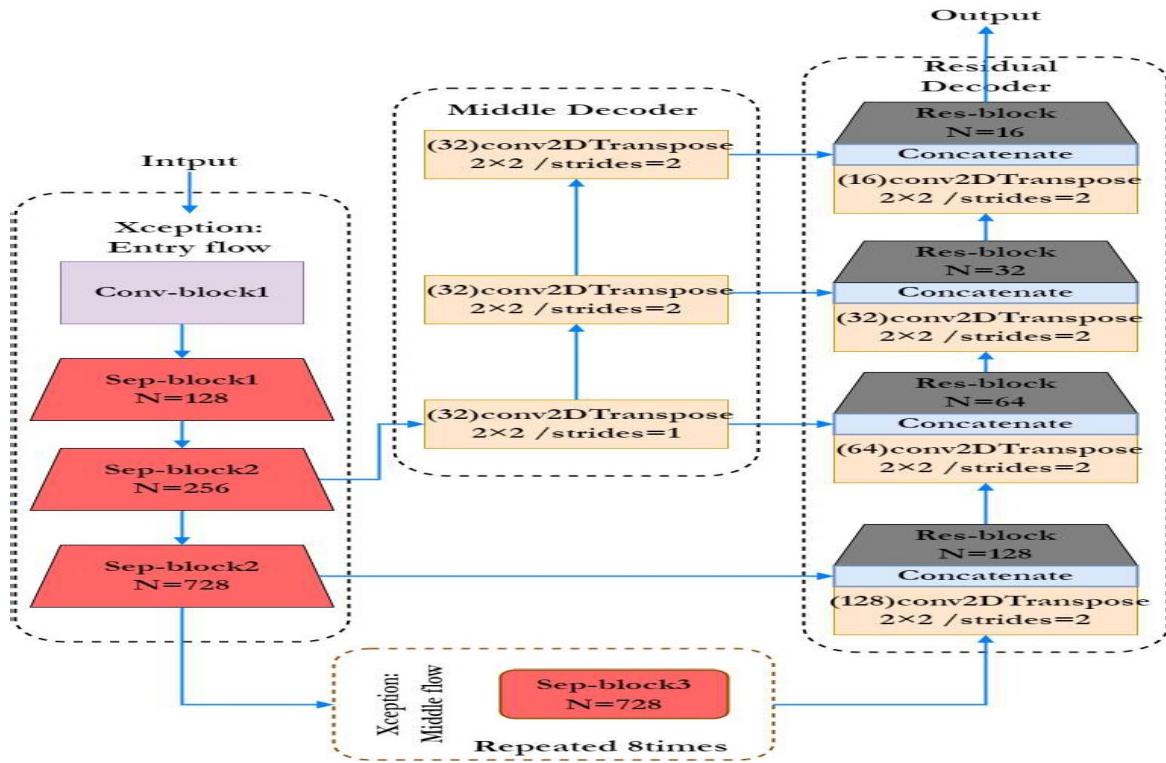


Table 1 . Experimental image Data set.

Class	Males	females	Total
Normal	31	40	71
spondylolisthesis	30	49	79
scoliosis	37	151	188

4.2. Metrics for Evaluation

To assess the performances, a number of widely used measures are used, such as precision, specificity, and accuracy. Intersection over Union (IoU) and Dice Similarity Coefficient (DSC). As stated in the following Eqn(1) and Eqn(2).

$$Pr = \frac{TP}{TP + FP}$$

$$Sp = \frac{TN}{TN + FP} \tag{1}$$

$$Acc = \frac{TP + TN}{TP + FP + TN + FN}$$

$$F1 = 2 \cdot \frac{Se \cdot Pr}{Se + Pr}$$

Where T P, TN, FP, and FN denote true positive, true negative, false positive and false negative, respectively.

$$IoU = \frac{A \cap B}{A \cup B},$$

$$DSC = \frac{2|A \cap B|}{|A| + |B|}, \tag{2}$$

where A and B represent pixel sets for the ground truths and their detection results, respectively

4. Experimental Results

Using transfer learning techniques, the first experiment involves pre-processing the datasets using the Keras application (i.e., normalising). Then, two distinct transfer learning strategies—TR1 and TR2—are applied. The layers chosen from the Xception architecture are regarded as feature extractors in transfer learning type 1 (TR1) and are frozen during the training stage. However, weights from the Xception architecture are used as beginning weights in transfer learning type 2 (TR2) and are retrained. Figure 5 and Figure 6 displays the DSC curves and average loss. This figure illustrates how switching from TR1 to TR2 transfer learning resulted in an increase in average DSC (0.8304 to 0.8726) and a drop in average loss (0.1709 to 0.1273) on the validation data. Because of this minimal similarity between the different datasets, the Xcep-ResUNet architecture performs better when the pre-trained architecture weights are updated. The segmentation result of normal, scoliosis, and spondylolisthesis are given in Figure 7. The performance comparisons of the proposed method on normal image data set are summarized in Table 2 and the Performance comparison of the proposed LW-RUNET method on abnormal (both

scoliosis and spondylolisthesis cases) dataset is given in Table 3.

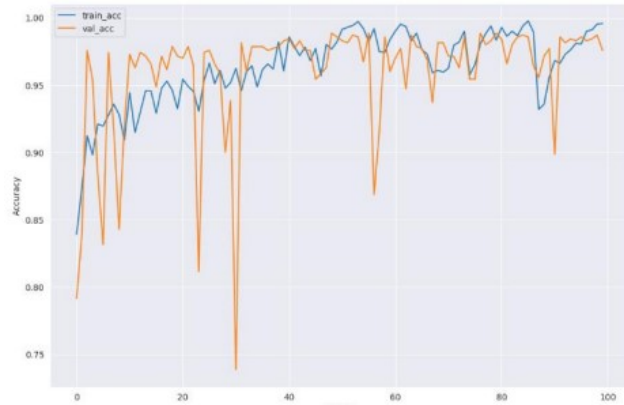


Fig 5 Training accuracy and validation accuracy in fine-tuning in two classes normal and scoliosis of our model.

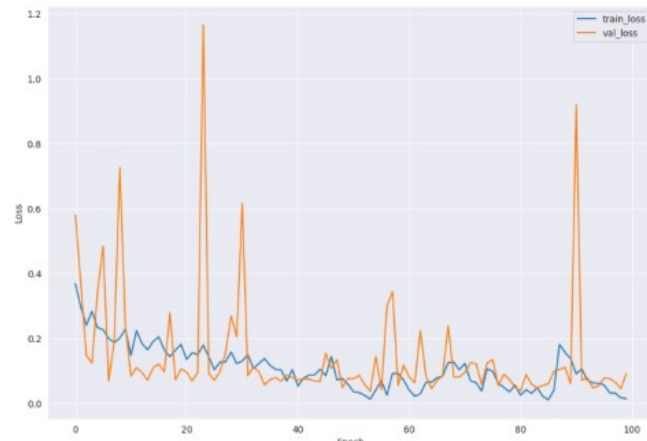


Fig 6 Training loss in and validation loss fine-tuning in two classes normal and scoliosis of our model.

Table 2. Comparison of the different segmentation methods on normal X-ray image dataset.

Method	IoU	DSC	Acc	Se	Sp	Pr
UNet	0.9328	0.9646	0.9903	0.9659	0.9948	0.9657
UNet++	0.9189	0.9562	0.9883	0.9627	0.9929	0.955
DeepLabV3	0.937	0.9666	0.9910	0.9755	0.9941	0.9601
ECANet	0.9326	0.9646	0.9675	0.9748	0.9545	0.9656
ResNet	0.9070	0.9490	0.9270	0.9480	0.9124	0.9434
DenseNet	0.8681	0.9281	0.989	0.9711	0.9903	0.8926
ChexNeXt	0.9100	0.9400	0.9534	0.9691	0.9423	0.9543
LW-RUNET	0.9471	0.9725	0.9928	0.9774	0.9954	0.9691

Table 3 Performance Comparison Of The Proposed LW-RUNET Method On Abnormal (Both Scoliosis And Spondylolisthesis Cases) Dataset

Metrics	Net	IoU	DSC	Acc	Se	Sp	Pr
IoU	UNet	0.9058	0.8608	0.8539	0.8734	0.8994	0.8787
	Unet++	0.8998	0.8672	0.8593	0.869	0.8921	0.8775
	DeepLabV3	0.8467	0.8203	0.8149	0.8165	0.8423	0.8281
	LW-RUNET	0.9155	0.8757	0.8696	0.8790	0.9077	0.8895
DSC	UNet	0.9492	0.9238	0.9201	0.9297	0.9459	0.9337
	Unet++	0.9455	0.9274	0.9230	0.9267	0.9413	0.9328
	DeepLabV3	0.9125	0.8975	0.8939	0.8930	0.9098	0.9013
	LW-RUNET	0.9546	0.9325	0.9293	0.9328	0.9503	0.9399

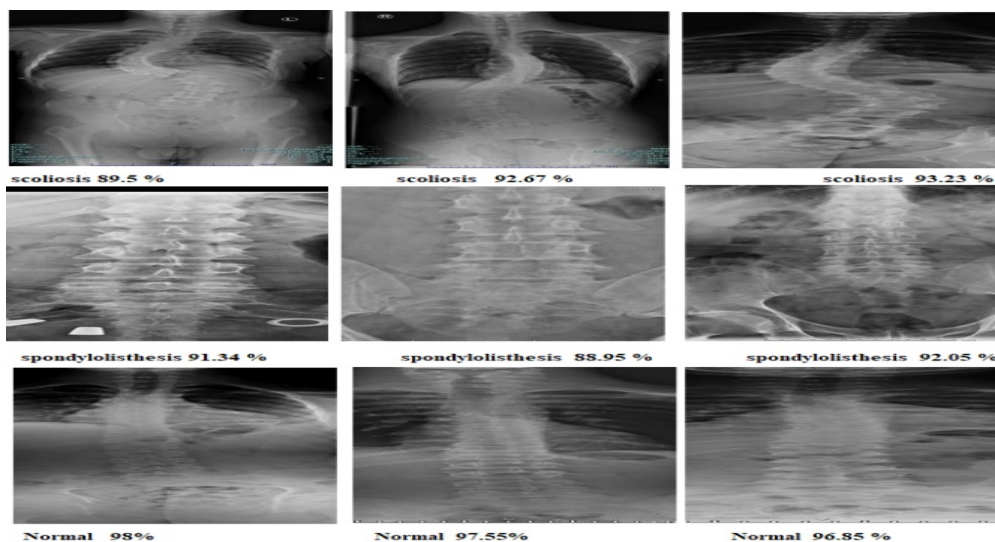


Figure 7 shows the segmentation results of the suggested method on three different classes, including normal, scoliosis, and spondylolisthesis.

The Comparative analysis of the proposed method and state-of-the-art methods on x-Ray image Data set is given in Table 4.

Table 4. Comparative Analysis Of The Proposed Method And State-Of-The-Art Methods On Given Data Set

Model	Accuracy	Recall	Precision	F1-score	AUC
Pham et al(2020)[21]	91.83	90.97	90.40	90.65	87.29
Chen et al(2020)[22]	93.54	92.73	93.35	93.01	90.50
Li et al(2022)[23]	97.22	96.63	97.01	96.81	95.64
Huang et al(2022)[24]	95.58	95.52	94.78	95.12	93.15
Zunti et al., (2020)[25]	95.75	94.91	95.08	94.96	93.36
Proposed (LW-ResUnet)	98.69	98.40	98.40	98.39	97.95

4.1 LOSS Function:

The cross entropy loss function is widely used in the field of semantic segmentation. The calculation of the cross entropy function LCE is shown in Eq.(9), and its value represents the difference between the true value and the predicted value, thus reflecting the accuracy of the model classification. It is given in Eqn(3)

$$L_{CE} = -[y \log \hat{y} + (1 - y) \log(1 - \log \hat{y})] \quad (3)$$

Among them, y represents the label value, and \hat{y} represents the predicted value of the model calculation result. The Dice Similarity Coefficient (DSC) can evaluate the similarity between two samples and has a good effect on dealing with the phenomenon of imbalanced elements in the two samples. The Dice loss function is a method that uses the value of DSC as the loss value. In image segmentation tasks, the proportion of abnormal pixels is very low, so the Dice loss function can be used to optimize the training process. The calculation of the loss value L , Dice is shown in Eq.(4).

$$L_{Dice} = 1 - 2 \times \frac{|P \cap T|}{|P| + |T|} = 1 - \frac{2 \times TP}{2 \times TP + FP + FN} \quad (4)$$

Among them, P represents the predicted part and T represents the true value.

Based on the characteristics of the segmentation task, the overall training loss L_{Total} is formed by combining cross entropy and Dice similarity coefficient loss function during the training process. The calculation is shown in Eq. (5):

$$L_{Total} = L_{CE} + L_{Dice} \quad (5)$$

5. CONCLUSIONS

Convolutional Neural Networks (CNN) have revolutionized deep learning for image categorization, particularly in the processing of X-ray images. Their ability to automatically extract hierarchical features from images enables accurate pattern recognition. To sum up, our goal is centered on improving the categorization of X-ray pictures of the vertebrae, which will greatly enhance the diagnostic potential of the medical industry. We are committed to the responsible and forward-thinking development of our model in order to improve patient care and medical decision-making as we traverse upcoming advances. This study discusses the early diagnosis

of scoliosis and spondylolisthesis disease using X-ray images. Currently, no direct test exists that can conclusively diagnose early kinds of AS; instead, medical imaging is needed, which results in an average seven to 10 year delay in diagnosis. Consequently, it is necessary to automatically identify the earliest AS signs by the analysis of medical photographs. This work leverages the Xception backbone for feature extraction in a Multi-Level Features Based Deep Convolutional Neural Network for Segmentation of Scoliosis and Spondylolisthesis utilising X-ray images. While the ResUNet decoder uses high-level features, the middle decoder uses middle features to get spatial information. To fine-tune the disease area, the suggested architecture integrates the ResUNet decoder characteristics with the proposed middle decoder features. Our suggested method outperforms previous deep learning models in terms of accuracy, as demonstrated by its evaluation using the X-ray picture database.

REFERENCES

- [1] W.H. Moon, W.K., Kim, S.J., Yi, A., B.L., Yun, N., Chang, J.M., Koo, H.R., M.Y. Kim, M.S. Bae, Breast cancer research and treatment, 138 (2013) 851-859; Ultrasonographic assessment of breast density.
- [2] Alessandrini, M. De Craene, O. Bernard, S. Giffard-Roisin, P. Allain, I. Waechter-Stehle, J. Weese, E. Saloux, H. Delingette, M. Sermesant, A pipeline for the generation of realistic 3D synthetic echocardiographic sequences: methodology and open-access database, , IEEE Transactions on Medical Imaging, 34 (2015) 1436-1451.
- [3] O Mattausch, E. Ren, M. Bajka, K. Vanhoey, O. Goksel),. Comparison of texture synthesis approaches for content generation in ultrasound simulation for training Medical Imaging 2017: Image-Guided Procedures, Robotic Interventions, and Modelling, SPIE, 2017, pp. 548-557.
- [4] Chen, X. Shi, Y. Zhang, D. Wu, M. Guizani,. Deep feature learning for medical image analysis with convolutional autoencoder neural network., IEEE Transactions on Big Data, 7 (2017) 750-758.
- [5] Aggarwal, V. Sounderajah, G. Martin, D.S. Ting, A. Karthikesalingam, D. King, H. Ashrafian, A. Darzi. Diagnostic accuracy of deep learning in medical imaging: a

- systematic review and meta-analysis NPJ digital medicine, 4 (2021) 65.
- [6] Aghamohammadi, R. Ranjbarzadeh, F. Naiemi, M. Mogharrebi, S. Dorosti, M. Bendechache TPCNN: two-path convolutional neural network for tumour and liver segmentation in CT images using a novel encoding strategy Expert Systems with Applications, 183 (2021) 115406.
- [7] Pang, J.H.D. Wong, W.L. Ng, and C.S. Chan, Semi-supervised GAN-based radiomics model for data augmentation in breast ultrasound mass categorisation Computer Methods and Programs in Biomedicine, 203 (2021) 106018.
- [8] Gao, Q. Jiang, B. Zhou, and D. Chen, Convolutional neural networks for computer-aided detection or diagnosis in medical image analysis: An overview. Mathematical Biosciences and Engineering, 16 (2019), 6536-6561
- [9] Rezazade Mehrizi, Mohammad; Scheek, D. H. and E. Ranschaert. Radiologists in the loop: The roles radiologists in the development of AI applications. (2021). European Radiology, 31(10), 7960–7968.
- [10] Jeon I, Kong E. Application of simultaneous 18F-FDG PET/MRI for evaluating residual lesion in pyogenic spine infection: a case report. Infect Chemother. 2020; 52(4): 626-633.
- [11] Radaelli D, Zanon M, Concato M, et al. Spine surgery and fat embolism syndrome. Defining the boundaries of medical accountability by hospital autopsy. Front Biosci (Landmark Ed). 2021; 26(12): 1760-1768.
- [12]. Altaf, F., Gibson, A., Dannawi, Z., Noordeen, H Adolescent Idiopathic Scoliosis. 2013 BMJ 346, 1527-1537.
- [13]. Jayachandran A, Dhanasekaran R (2017) Multi class brain tumor classification of MRI images using hybrid structure descriptor and fuzzy logic based RBF kernel SVM. Iran J Fuzzy Syst 14(3):41–54.
- [14]. Mahiba C, Jayachandran A (2019) Severity analysis of diabetic retinopathy in retinal images using hybrid structure descriptor and modified CNNs. Meas 135:762–767.
- [15]. Jones C. F. and Clarke E. C., Engineering approaches to understanding mechanisms of spinal column injury leading to spinal cord injury, Clinical Biomechanics. (2019) 64, 69–81.
- [16] Mangone M, Paoloni M, Santilli V, Agostini F, Bernetti A, Colombo T, et al. Based on non-invasive rasterstereography analysis, supervised and unsupervised learning was used to categorise individuals with scoliosis and healthy participants. PLOS ONE. 16(12):e0261511 in 2021. PMID: 34941924.
- [17]. Wang H, Zhang T, Cheung KMC, Shea GKH., Application of deep learning to spinal radiographs to predict progression in adolescent idiopathic scoliosis at first clinic visit: Clinical Medicine Online. 2021; 42:101220. PMID: 34901796;
- [18]. Jayachandran A, Shunmugarathinam G, Perumal TSR (2023) Retinal vessels segmentation of colour fundus images using two stages cascades convolutional neural networks. J Ambient Intell Hum Comput Secur 14(7):9305–9315
- [19] Jayachandran A , Sreekesh Namboodiri T(2020) Multi-class skin lesions classification system using probability map based region growing and DCNN. Int.J Comput Intell Syst 13(1):77–84.
- [20] Jesu Prabhu A, Jayachandran A (2018) Mixture model segmentation system for parasagittal meningioma brain tumor classification based on hybrid feature vector. J Med Syst 42:12
- [21] Pham, H. H., Le, T. T., Tran, D. Q., Ngo, D. T., & Nguyen, H. Q. (2020). Interpreting chest X-rays via CNNs that exploit hierarchical disease dependencies and uncertainty labels (arXiv:1911.06475). arXiv. <http://arxiv.org/abs/1911.06475>
- [22] Chen, H., Miao, S., Xu, D., Hager, G. D., & Harrison, A. P. (2020). Deep Hierarchical Multi-Label Classification Applied to Chest X-Ray Abnormality Taxonomies (arXiv:2009.05609). arXiv. <http://arxiv.org/abs/2009.05609>
- [23] Li, L., Cao, P., Yang, J., & Zaiane, O. R. (2022). Modeling global and local label correlation with graph convolutional networks for multi-label chest X-ray image classification. Medical & Biological Engineering & Computing, 60(9), 2567–2588.
- [24]. Huang, G.-H., Fu, Q.-J., Gu, M.-Z., Lu, N.-H., Liu, K.-Y., & Chen, T.-B. (2022). Deep Transfer Learning for the Multilabel Classification of Chest X-ray Images. Diagnostics, 12(6), 1457.

- [25].Zunti G,Park E H,"Early detection of ankylosing spondylitis using texture features and statistical machine learning, and deep learning, with some patient age analysis", Computerized Medical Imaging and Graphics 82 (2020) 101718.Issues and Challenges”, Computational Methods in Engineering, 30:1863–1895.